



## Deformation and heat treatment ability of three-layer 6009/7050/6009 Al alloy clad slab prepared by direct-chill casting

Guang-yuan YAN, Feng MAO, Zhi-qiang CAO, Ting-ju LI, Tong-min WANG

Key Laboratory of Solidification Control and Digital Preparation Technology (Liaoning Province),  
School of Materials Science and Engineering, Dalian University of Technology, Dalian 116024, China

Received 12 August 2016; accepted 24 March 2017

**Abstract:** Three-layer 6009/7050/6009 aluminum alloy clad slab was fabricated by an innovative direct-chill casting process. To study the response of the clad slab to plastic deformation and heat treatments, homogenization annealing, hot rolling, solution and aging were successively performed on the as-cast 6009/7050/6009 clad samples. The results revealed that excellent metallurgical bonding between 7050 alloy layer and 6009 alloy layer was achieved under optimal parameters. The clad ratio obviously decreased when the annealed sample was rolled to 55% hot reduction level, and then changed slightly with further rolling. Furthermore, the content of rodlike Zn-rich phases increased significantly in 7050 alloy layer in the homogenized clad samples after rolling at 55%, 65% and 75% hot reduction levels, and the higher level of hot reduction resulted in narrower diffusion layer. Subsequent solution and aging significantly improved the hardness in 7050 alloy layer, interfaces and 6009 alloy layers of the rolled samples except for the thin side for the 75% hot reduction sample.

**Key words:** aluminum alloy; three-layer clad slab; direct-chill casting; plastic deformation; heat treatment

### 1 Introduction

Metal matrix composites particularly offer the intrinsic advantages of additional properties which benefit from the addition of dispersed particles [1], fibers [2], or layers [3]. As described by KOCICH et al [4], the development of new composites becomes more and more important in materials research field. Among them, the multilayer composite plates are of significant interest for application in many industrial fields, which results from their comprehensive physical, chemical and mechanical properties [5]. Multilayer composite materials were usually prepared by centrifugal casting [6] and laser cladding [7]. Besides, explosive welding was used to prepare magnesium AZ31–aluminum 7075 composite, aluminum and copper plates and other metal plates [8–10]. Furthermore, the similar/dissimilar light metal sheets, Mg/Al clad and stainless steel/aluminum sheet have been developed by diffusion bonding [11–13]. Recently, several new forming technologies have been applied to manufacturing clad composites. For example, the 6xxx/5xxx/6xxx aluminum

clad sheets, 7075 Al/Mg–Gd–Y–Zr/7075 Al laminated composite and Mg/Al laminated composite were fabricated through rolling bonding [14–16]. Moreover, KOCICH et al [3,4] used the rotary swaging process to fabricate the clad composites, though the non-uniform strain distribution through the cross-section of a swaged rod was its potential disadvantage.

However, the above processes have the problem of low bonding strength between different metal layers. The direct-chill casting is an ideal method for producing multilayer clad slab as it can solve the problem of low bonding strength, as well as its lower cost and high productivity. The Novelis fusion process was used to manufacture the clad ingot [17]. SUN et al [18], JIANG et al [19] and LIU et al [20] prepared the Al–Si alloy and Al–Mn alloy clad aluminum by direct-chill continuous casting. What's more, in our previous work the 6009/7050 clad ingot developed by direct-chill casting was reported, and its characteristics evolution was also investigated [21,22].

The three-layer 6009/7050/6009 clad slab using 6009 alloys as protective layers, would be expected to improve the corrosion resistance of the high-strength

7050 alloys as well as formability. In this work, the 6009/7050/6009 three-layer clad slab was produced by an innovative direct-chill casting process. More attention was paid to the plastic deformation and heat treatment behaviors of the 6009/7050/6009 three-layer clad slabs, owing to the importance in the potential use in airplane industries of this clad slab and similar composite ingots in commercial applications. The evolution of microstructures, composition distribution and mechanical properties of the as-cast clad slab after plastic deformation and heat treatments were studied in details.

## 2 Experimental

### 2.1 Materials and ingot preparation

The experimental materials including 7050 alloy melt and 6009 alloy melt were prepared separately by melting the commercial pure aluminum, zinc, copper, magnesium, manganese, crystalline Si and Al-4%Zr master alloy at appropriate ratios in their respective pot resistance furnaces. Fluorometric analysis was used to measure the chemical compositions of the 6009 alloy layer and 7050 alloy layer and the results were presented in Table 1. The three-layer 6009/7050/6009 clad ingot was prepared by an innovative direct-chill casting process. Figure 1 reveals the schematic illustration of experimental apparatus. The results demonstrated that two same water-cooled baffles were placed in the mold in parallel and divided the mold inside into three sections symmetrically. The pouring process and solidification process of the 6009/7050/6009 clad ingot resemble that of 6009/7050 bimetal slab, mentioned in our previous work [21]. The three-layer 6009/7050/6009 aluminum clad slab (150 mm × 120 mm × 100 mm) was finally obtained. The optimized experimental parameters were gained after a battery of systematic experiments: the pouring temperatures of 6009 melt and 7050 melt were 715 °C and 720 °C, respectively, the drawing speeds of two water-cooled baffles were both 70 mm/min, and the cooling water flow rates of two water-cooled baffles were both 140 L/h.

**Table 1** Chemical compositions of experimental alloys (mass fraction, %)

Alloy	Zn	Cu	Mg	Si	Fe	Zr	Mn	Cr	Al
7050	6.57	2.04	1.97	0.093	0.114	0.09	0.003	0.021	Bal.
6009	–	–	0.41	0.792	0.134	–	0.004	0.018	Bal.

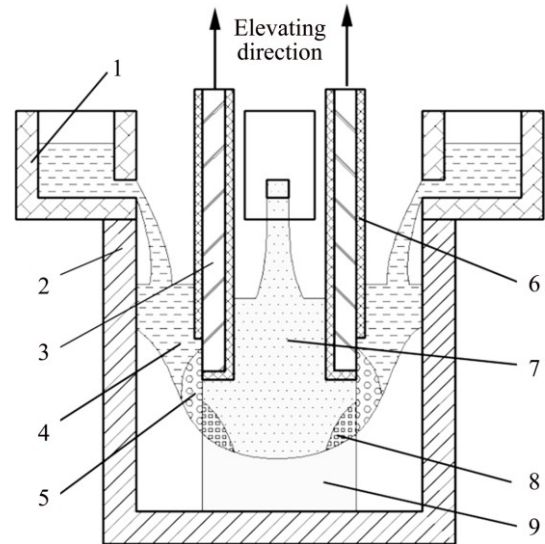


**Fig. 1** Schematic illustration of modified direct-chill casting process: 1—Hot top; 2—Mold; 3—Water cooled baffle; 4—6009 alloy melt; 5—6009 alloy semisolid shell; 6—Heat insulation layer; 7—7050 alloy melt; 8—7050 alloy semisolid shell; 9—Clad slab

### 2.2 Plastic deformation and heat treatments

A test sample with a length of 130 mm, a width of 80 mm and a height of 50 mm, was prepared by wire-electrode cutting technique from the as-cast three-layer 6009/7050/6009 aluminum clad slab and the thickness for the thin 6009 layer, 7050 layer and thick 6009 layer of the test sample was 8, 60 and 12 mm, respectively. In this work, the interfacial region on 8 mm 6009 layer side was called the interface for the thin side, while the interfacial region on 12 mm thick 6009 layer side was called the interface for the thick side. Figure 2 shows the heat treatment and plastic deformation

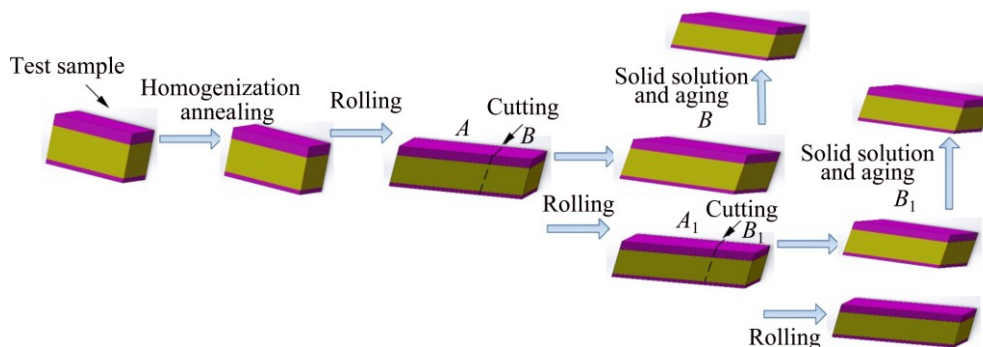


**Fig. 2** Schematic illustration of heat treatment and plastic deformation procedures of 6009/7050/6009 clad samples

procedures of the clad test samples. The homogenization annealing process was 460 °C for 24 h. The homogenized 80 mm thick slab was then subjected to subsequent hot rolling processes with a 55% hot reduction (55% HR) at (450±10) °C, and its thickness became 36 mm. This process was sequentially repeated to produce 65% hot reduction (65% HR) sample and 75% hot reduction (75% HR) sample, and the corresponding thicknesses of the clad samples were 28 and 20 mm, respectively. The 55% HR, 65% HR and 75% HR samples were then solution treated at 477 °C for 90 min, followed by 60 °C water-immersion quenching. Subsequent artificial secondary aging treatments were selected as 121 °C for 6 h and then 177 °C for 8 h. Six test samples were thus acquired after solution and aging treatments (SA): 55% HR, 65% HR, 75% HR, 55% HR+SA, 65% HR + SA, and 75% HR + SA.

### 2.3 Structure observation, composition analysis and properties test

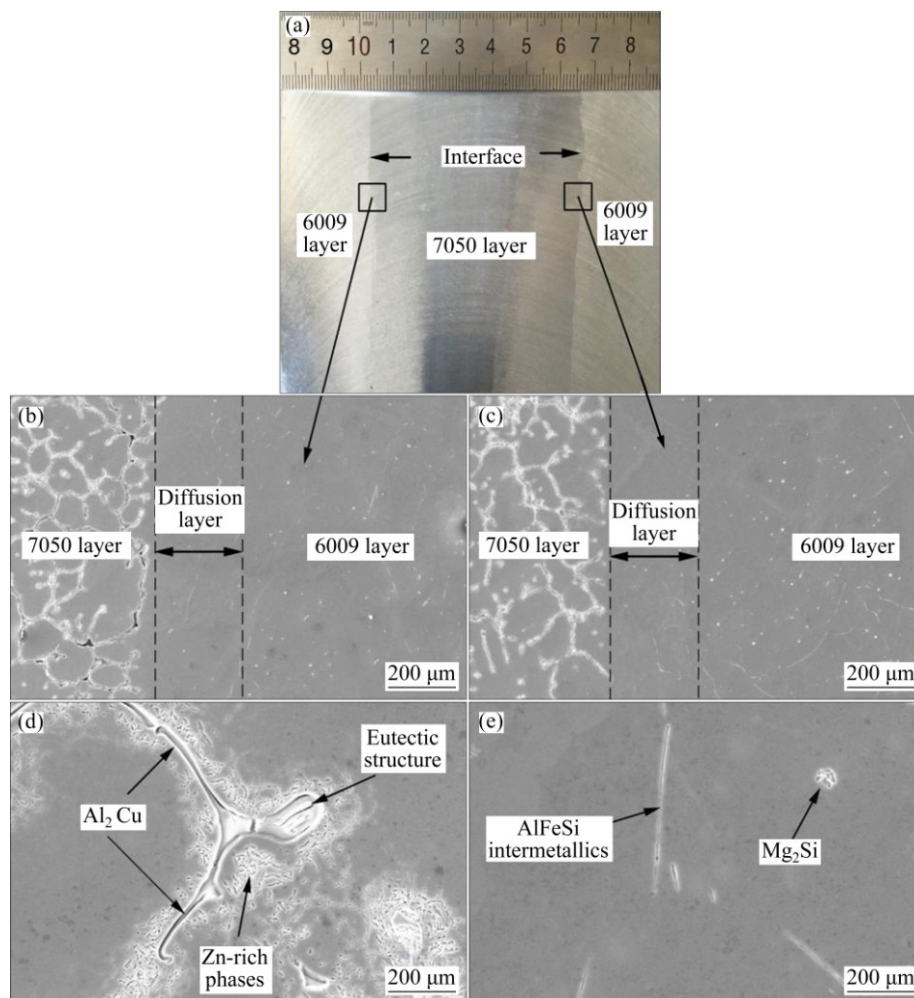
Milling was performed on the cross section of the as-cast clad slab to obtain the macrostructure image.

Scanning electron microscope (SEM, Zeiss supra 55), conducted in secondary electron mode operated at 15 kV, was used to investigate the microstructure of the test samples. To analyze the composition distribution, electron microprobe (EPMA–1600) analysis operated at 15 kV was carried out in the interfacial regions of the clad samples. The Vickers hardness measurements were performed in the interfacial regions of the test samples with a load of 50 g for 15 s. The thickness of every layer for the clad samples was measured by a digital display vernier caliper. The repeated number of measures for every layer was 15 and the average value was considered as the thickness for every layer.

## 3 Results and discussion

### 3.1 Microstructure, composition and hardness of as-cast clad

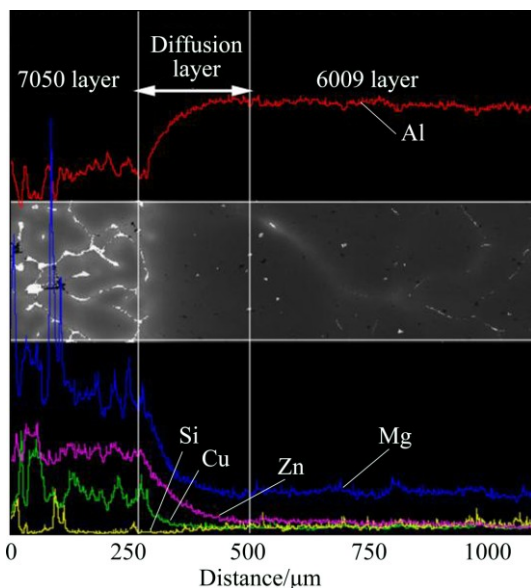
Figure 3 shows the as-cast macrostructure and microstructures of the three-layer 6009/7050/6009 clad slab. Figure 3(a) reveals that the clad slab is distinctly separated by two clean interfaces into the middle 7050



**Fig. 3** Macrostructure (a), microstructures in left (b) and right (c) interfacial regions of clad slab, SEM images on 7050 alloy side (d) and 6009 alloy side (e) of as-cast 6009/7050/6009 clad slab at high magnification

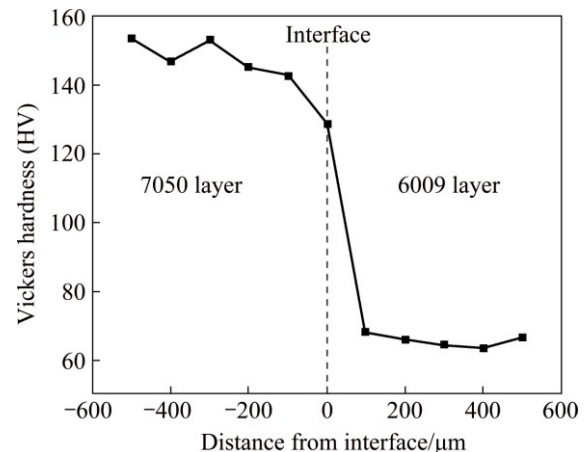
alloy layer and bilateral 6009 alloy layers due to the difference between respective surface brightness after grinding. Figures 3(b) and (c) reveal the microstructures at the left and right interfaces of the as-cast clad slab, respectively. Figure 3(d) shows the SEM image of the 7050 alloy layer at high magnification. The results indicated that lamellar  $\alpha(\text{Al}) + T(\text{AlZnMgCu})$  eutectic structure and plate-like  $\text{Al}_2\text{Cu}$  phases were distributed at grain boundary, while rodlike Zn-rich phases precipitated within the grains. While, the SEM image of the 6009 alloy layer at high magnification is presented in Fig. 3(e). It was found that two kinds of second phases precipitated in  $\alpha(\text{Al})$ : plate-like  $\text{AlFeSi}$  intermetallics and cluster-like  $\text{Mg}_2\text{Si}$  phases. This also demonstrated that a good metallurgical bonding between the 7050 alloy layer and 6009 alloy layer was obtained because there were few casting defects and no discontinuities in both left and right interfacial regions.

Figure 4 demonstrates the composition variations of the Zn, Mg, Cu and Si elements across the interface of the as-cast clad slab. The contents of Mg, Zn and Cu decreased gradually across the interface from 7050 layer to 6009 layer while the Si element showed inverse trend. The composition variation curves in diffusion layer and 6009 layer were smoother than that of 7050 layer, indicating that the diffusion layer and 6009 layer achieved more uniform elements distribution. What's more, the content variation of Zn was chosen to define the diffusion layer thickness in the present study. This average diffusion layer thickness for the three-layer clad slab was found to be about 250  $\mu\text{m}$ . Furthermore, the diffusion layer should be primary  $\alpha(\text{Al})$  layer that primarily contained Zn and Mg as well as small amounts of Cu and Si.



**Fig. 4** EPMA line analysis of elements Zn, Mg, Cu and Si in interfacial region of as-cast 6009/7050/6009 clad slab

The Vickers hardness of the as-cast three-layer clad material was measured across the interface, and the results are presented in Fig. 5. It was seen that the average hardness for 7050 layer was about HV 150, while it was around HV 60 for the 6009 layer. The average Vickers hardness at the interface was measured to be nearly HV 125. Solution strengthening by diffused atoms might result in this improved hardness at interface, which was higher than that of the 6009 alloy layer.



**Fig. 5** Distribution of Vickers hardness across interfacial region of as-cast 6009/7050/6009 clad slab

### 3.2 Plastic deformation and heat treatments

#### 3.2.1 Clad ratio variations of homogenized clad during hot rolling

CHAUDHARI and ACOFF [23] reported that during hot rolling, the thickness ratio or clad ratio of constituent layers was a function of the mechanical properties of the constituent layers, rolling parameters and initial thickness ratio of these layers. In the present study, clad ratio was defined as the ratio of the 6009 layer thickness to the total sample thickness. Figure 6 displays the variation of the clad ratio and the thickness of 6009 layer in the clad slab after hot rolling process. It could be seen that the thickness of 6009 layer on both the thin side and the thick side decreased with the reduction of the sample thickness. When the sample was rolled from 80 to 36 mm sample, significant decrease occurred in the clad ratio on both thin side and thick side. The variations of the clad ratio on the thin side and thick side in the samples after rolling indicated that the thickness reductions of the 6009 layer and 7050 layer were inhomogeneous during the rolling processes. One thing to worth mentioning is that the resistance to plastic flow of 7050 alloy should be larger than that of 6009 alloy when the rolling temperature is 450  $^{\circ}\text{C}$ , so the softer 6009 layers accommodates a greater proportion of the plastic strain than 7050 layer during rolling. Therefore, the clad ratios on both thin side and thick side are

reduced during hot rolling to 36 mm sample. However, the clad ratios on both the thin side and the thick side of the sample showed a slight increase with the further reduction of the sample thickness to 28 mm. This improved clad ratio might be attributed to work hardening, making the resistance to plastic flow of 6009 layer increased and larger than that of 7050 layer. In addition, when the sample continued to be rolled to 20 mm, the clad ratio on the thick side kept increasing but the inverse trend occurred for that of the thin side. The plastic deformation at 450 °C was a competitive process of work hardening and dynamic softening such as dynamic recovery or dynamic recrystallization. At the beginning of plastic deformation, the increased dislocation density leads to the increase of the resistance to plastic flow in 6009 layer and 7050 layer, and the resistance to plastic flow in 6009 layer should increase faster than that in 7050 layer according to the above analysis. DENG et al [24] described that as the deformation proceeded, the dynamic softening such as dynamic recovery or dynamic recrystallization might occur, which could offset or partially offset the effect of work hardening, and then the resistance to plastic flow remained unchanged or fell to some extent. It could be calculated from Fig. 6 that the 6009 layer on the thin side suffered from a greater thickness reduction (91.2%) than that of the thick side (87.4%). This greater thickness reduction might more easily induce the occurrence of dynamic recovery or dynamic recrystallization in 6009 layer at the same deformation temperature, which resulted in the rapid decrease of the resistance to plastic flow in the 6009 layer on the thin side of the clad. This was why the clad ratio on the thin side showed decreased trend again when the sample continued to be rolled to 20 mm, as presented in Fig. 6.

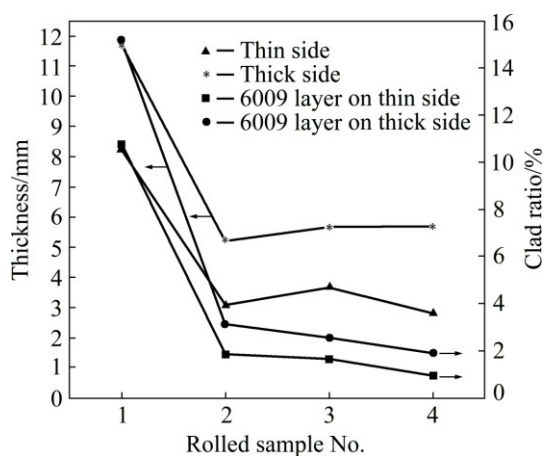


**Fig. 6** Variation of clad ratio and 6009 clad layer thickness on thin side and thick side in homogenized 6009/7050/6009 clad slab after rolling process (Sample 1: As-cast, 80 mm; Sample 2: 55% HR, 36 mm; Sample 3: 65% HR, 28 mm; Sample 4: 75% HR, 20 mm)

### 3.2.2 Microstructures of homogenized clad after hot rolling

The microstructures along the deformation direction of the homogenized 6009/7050/6009 clad samples after rolling to 36 mm (55% HR) are presented in Fig. 7. The microstructures in the interfacial region on the thin side and the thick side of the 6009/7050/6009 clad samples are respectively shown in Figs. 7(a) and (b). The results revealed that the two interfaces were still distinct and the three-layer structures in as-cast state were maintained after successive homogenization annealing and hot rolling processes. It could be seen from Fig. 7(a) that obvious plastic deformation along the rolling direction occurred in both 7050 layer and 6009 layer. For 7050 layer, most of the precipitated phases at the grain boundary in as-cast state were fragmented and parts of them were dissolved. Moreover, the fiber-like structures were formed in both 7050 layer and 6009 layer, and the  $\alpha(\text{Al})$  grains and precipitated phase particle structures were stretched along the deformation direction. As shown in Fig. 7(b), most of the precipitated phases fade away in both 7050 and 6009 layers on the thick side of the homogenized clad after rolling. Figures 7(c) and (d) show the SEM images of 7050 layer on the thin side and the thick side respectively of the homogenized clad after rolling at high magnification. The results revealed that most of the  $\alpha(\text{Al}) + T(\text{AlZnMgCu})$  eutectic structure and  $\text{Al}_2\text{Cu}$  phases were fragmented and dissolved. The residual phases at the grain boundary were mainly nubbly  $\text{Al}_2\text{Cu}$  phases. Furthermore, the amount of the residual  $\text{Al}_2\text{Cu}$  phases on the thin side (Fig. 7(c)) was greater than that on thick side (Fig. 7(d)). In addition, the content of rodlike Zn-rich phases precipitated within the grains in 7050 layer increased markedly, compared with that of the as-cast state. The SEM images of 6009 layer on the thin side and the thick side of the homogenized clad after rolling at high magnification are respectively shown in Figs. 7(e) and (f). The results suggested that the amount of  $\text{Mg}_2\text{Si}$  phases showed distinct increase and the  $\text{AlFeSi}$  phases cracked into finer needle-like particles. Figures 7(g) and (h) present the SEM images of the interfaces on the thin side and the thick side at high magnification, respectively. After rolling, the needle-like phases and globular phases precipitated at the interfaces of the 6009/7050/6009 clad sample. EPMA measurements suggest the composition of plate-like phases is 75.836% Al and 24.089% Si, while the EDS analysis shows that the composition of globular phases is 67.81% Al and 31.89% Si. These results indicated that the needle-like phases and globular phases precipitated at the interfaces were all  $\text{AlSi}$  intermetallics.

### 3.2.3 Microstructures of rolled clad after solution and aging

The typical microstructures of the rolled 6009/7050/

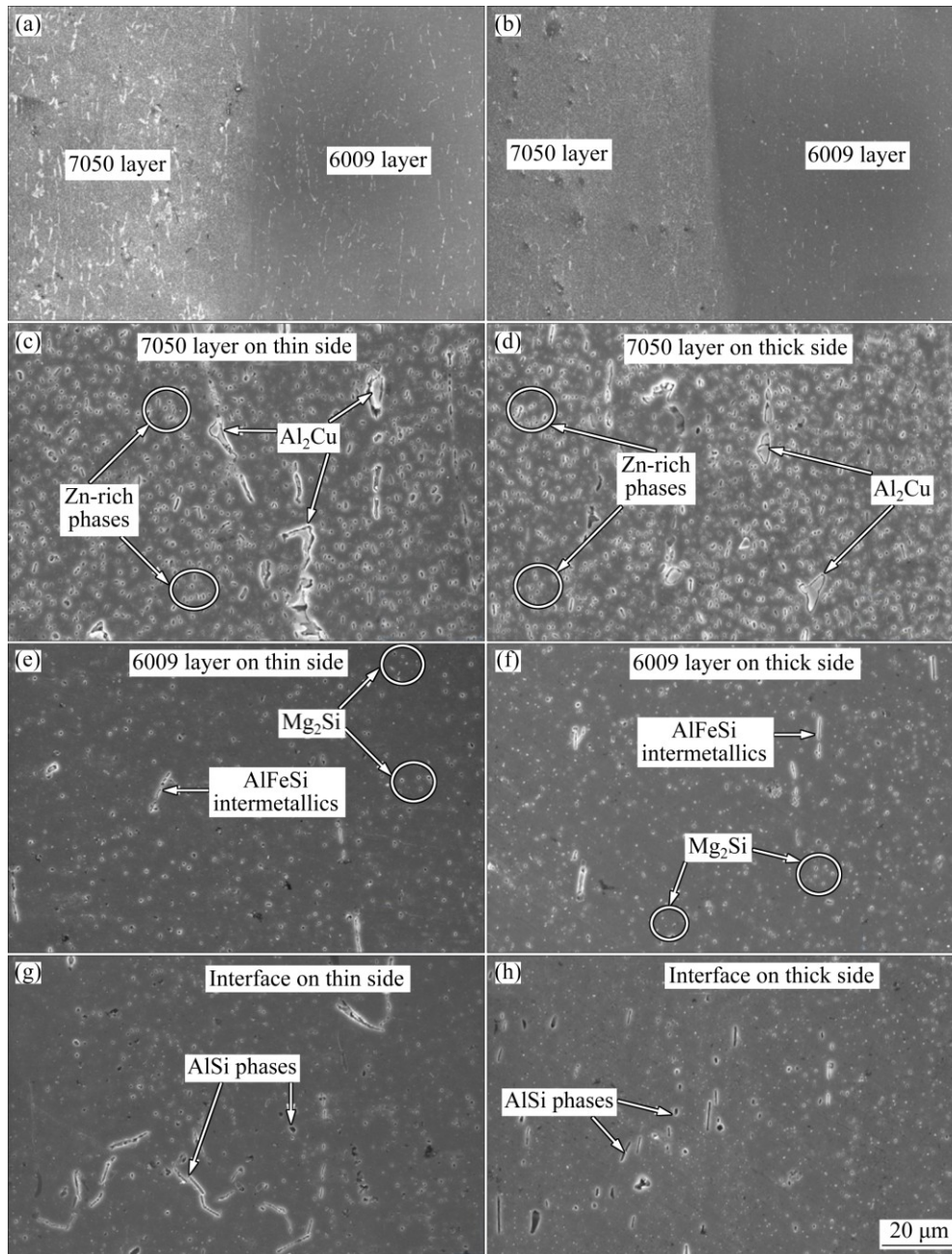


**Fig. 7** Secondary electron SEM images of interfacial region on thin side (a) and thick side (b) of homogenized 6009/7050/6009 clad samples after rolling to 36 mm (55% HR); SEM images of 7050 layer (c), 6009 layer (e) and interface (g) on thin side at high magnification; and SEM images of 7050 layer (d), 6009 layer (f) and interface (h) on thick side at high magnification

6009 clad samples (75% HR) after subsequent solution and aging are presented in Fig. 8. It could be seen from Figs. 8(a) and (b) that the interfaces on the thin side and the thick side of the sample were still clear after solution and aging, and the lamellar structures in as-cast and rolled states were maintained. Figures 8(c) and (d) suggested that the Zn-rich phases in 7050 layer were dissolved and disappeared after solution and aging, and the residual phases were only  $\text{Al}_2\text{Cu}$  phases. As shown in Figs. 8(e)–(h), no obvious changes could be found in the 6009 layers and interfaces of the clad sample after

solution and aging compared to the rolled state.

### 3.2.4 Composition analysis of rolled clad after solution and aging

Figure 9(a) shows the diffusion layer thickness variations during the as-casting, hot rolling, and subsequent solution and aging of the 6009/7050/6009 clad samples. For the homogenized samples after rolling, the lower data points indicated the diffusion layer thickness values on the thin side of the clad samples, while the upper data points reflected the diffusion layer thickness on the thick side. With the clad sample rolled

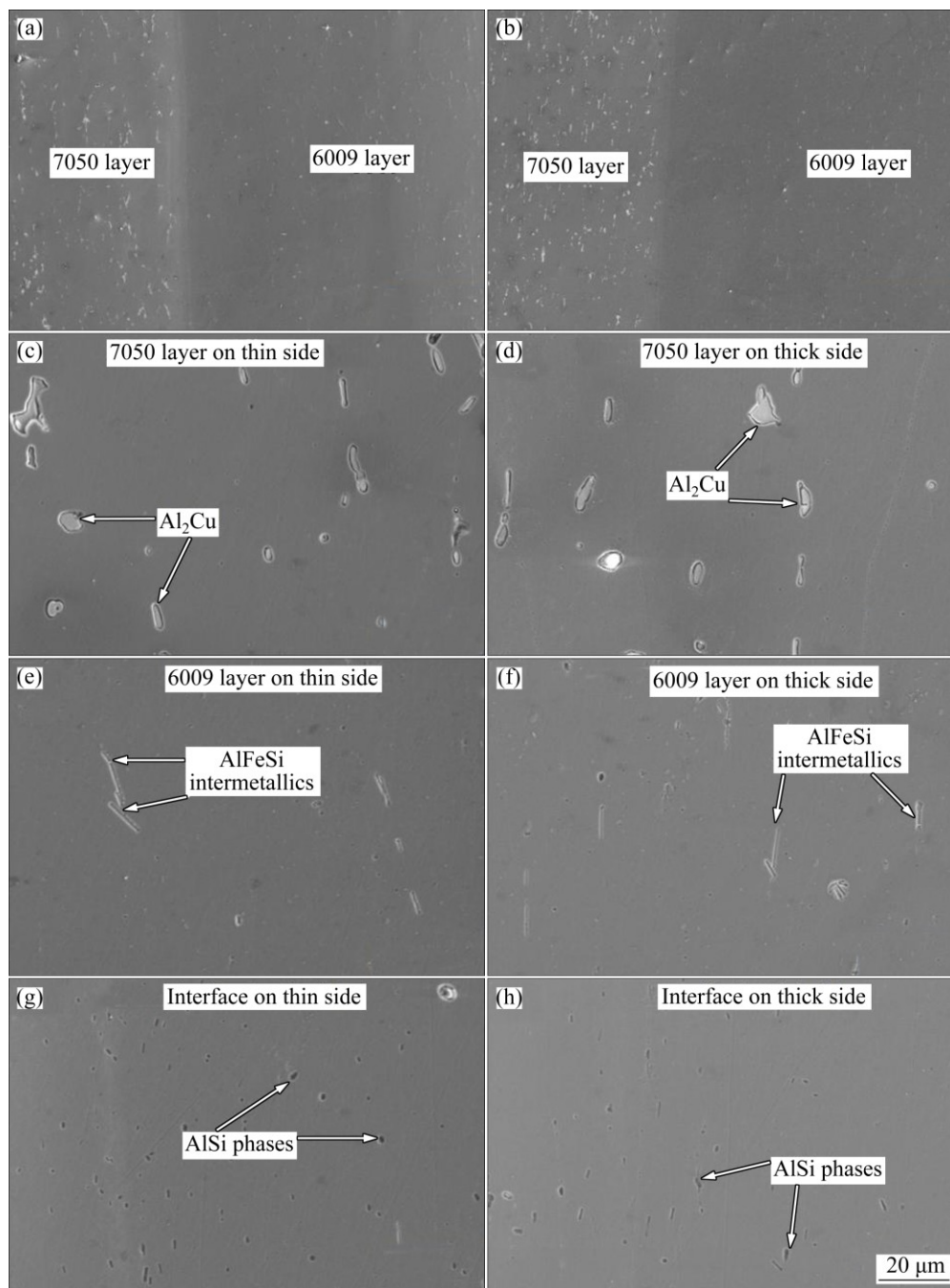


**Fig. 8** Secondary electron SEM images of interfacial on thin side (a) and thick side (b) of rolled 6009/7050/6009 clad samples (75% HR) after solution and aging; SEM images of 7050 layer (c), 6009 layer (e) and interface (g) on thin side at high magnification; and SEM images of 7050 layer (d), 6009 layer (f) and interface (h) on thick side at high magnification

to 20 mm (75% HR), the diffusion layer thickness on the thin side and the thick side decreased to 160 and 190  $\mu\text{m}$ , respectively. The significant diffusion layer thickness increase was observed for both thin side and thick side of the rolled samples after subsequent solution and aging. Furthermore, the diffusion layer thickness in the aged samples fell with the reduction of the clad sample thickness. Line scan of elements using EPMA was performed in order to characterize the distribution of Zn,

Cu, Mg and Si elements across the bonding interface. The typical elements distributions in the interfacial region on the thin side and the thick side of the aged clad samples are presented in Figs. 9(b) and (c), respectively. More flat profiles suggested that compared to as-cast state, the Zn, Mg, Cu and Si elements in the interfacial regions received more uniform distributions after successive homogenization annealing, rolling, solution and aging.

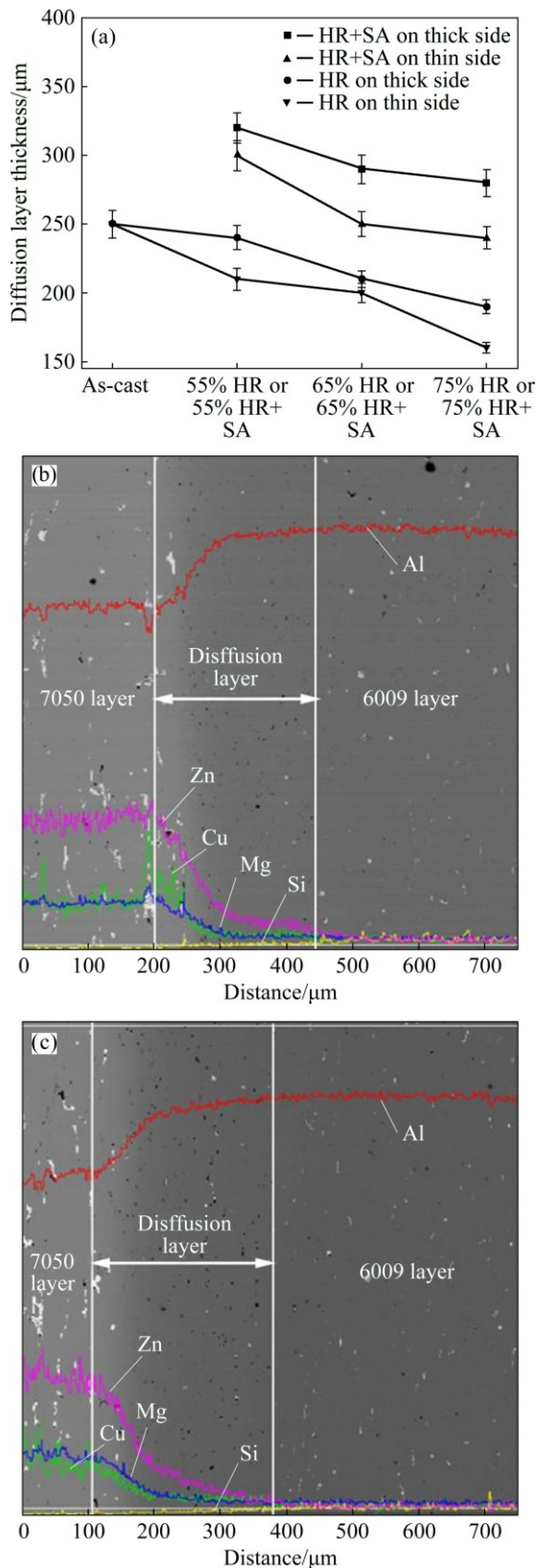


**Fig. 9** Diffusion layer thickness plot of 6009/7050/6009 clad samples (a), EPMA line analysis on thin side (b) and thick side (c) of rolled clad sample (75% HR) after solution and aging (The distribution of Zn, Cu, Mg and Si elements and the backscattered micrograph in interfacial region)

The diffusion layer thickness during hot rolling depends on the competitive factors: atoms diffusion and strain magnitude. The atoms diffusion accompanying with hot rolling makes the diffusion layer thickness larger while the plastic strain causes the inverse trend. If the effect of the plastic strain was larger than that of the atoms diffusion, the final thickness of diffusion layer would decrease. In this work, it is noted that the effect of the plastic strain should be larger than that of the atoms diffusion due to the final diffusion layer thickness decreasing after rolling on both the thin side and the thick side. Besides, the diffusion layer thickness on the thin side was smaller than that on the thick side of the clad, indicating that diffusion layer on the thin side received greater plastic strain than that on the thick side of the clad, due to their same homogenization annealing and rolling conditions. Furthermore, the diffusion layer thickness after solution and aging was larger than that of the rolled sample as a result of the occurrence of elements diffusion across the interface during solution and aging treatment.

### 3.2.5 Hardness variations of rolled clad after solution and aging

Figure 10 demonstrates the Vickers microhardness distributions across the interfaces on the thin side and the thick side of the homogenization-annealing samples after various rolling and heat treatments. The result revealed that the as-cast layered characteristics of the microhardness distribution were retained. Compared to the as-cast sample, the hardness decreased significantly after subsequent homogenization annealing and hot rolling to 36 mm (55% HR) on the thin side of the clad sample, as shown in Fig. 10(a). Then, the average hardnesses of the 7050 layer and interface, however, increased markedly after the further rolling, but had small change in the 6009 layer hardness of 65% HR specimen and 75% HR specimen, in which the average hardness of the 7050 layer and interface in 75% HR specimen was higher than that of 65% HR specimen. Furthermore, the solution and aging treatment raised the hardness of the 55% HR, 65% HR and 75% HR specimens, the hardness of both 55% HR + SA and 65% HR + SA specimens was much higher than that of the 75% HR + SA specimen. The average hardness values of 7050 layer, interface and 6009 layer on the thin side of 65% HR+SA specimen were HV 163, HV 130 and HV 90, respectively. Figure 10(b) presents the microhardness variations in the interfacial region on the thick side of the clad samples. The results suggested that the hardness values of all the homogenized samples after rolling, such as 75% HR, 65% HR and 55% HR samples, were much lower than that of as-cast sample. Moreover, slight increase in average hardness occurred in 7050 layer and

interface with the sample thickness decreasing during hot rolling, but the average hardness of 6009 layer showed small change. After subsequent solution and aging, the average hardness of 7050 layer, interface and 6009 layer increased significantly. Furthermore, there was small difference in hardness among 75% HR, 65% HR and 55% HR samples. The average hardness of 7050 layer, interface and 6009 layer on the thick side of 65% HR + SA specimen were HV 155, HV 140 and HV 85, respectively.

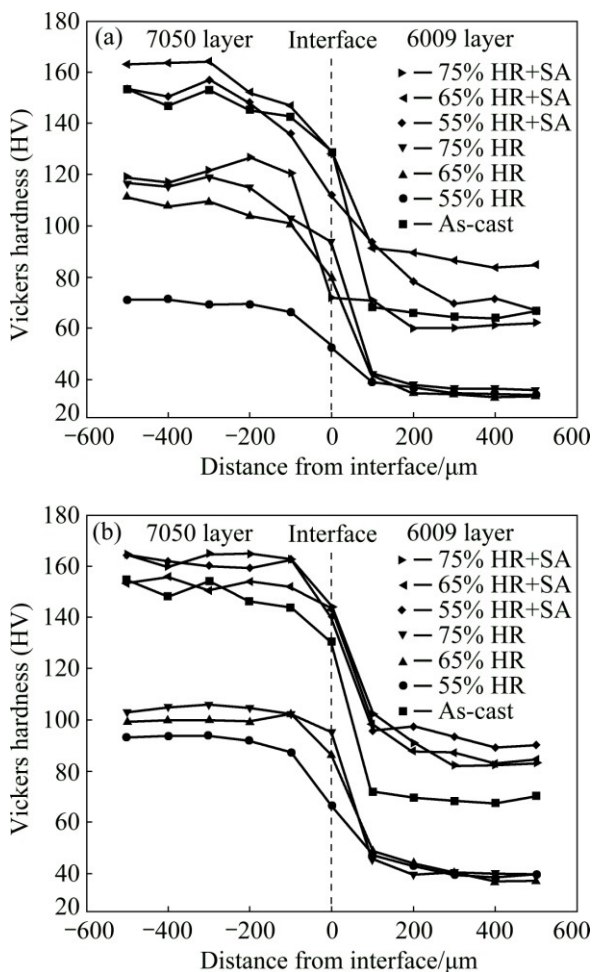


**Fig. 10** Microhardness distributions across interfaces on thin side (a) and thick side (b) of 6009/7050/6009 clad samples under various rolling and heat treatments

During homogenization annealing, the dissolution of reinforced phases such as  $T(\text{AlZnMgCu})$  phase was considered as the dominating softening mechanism of 7050 alloy layer, while the dominating softening mechanism of 6009 alloy layer might be grain coarsening, which weakened the dislocation reinforcement at the grain boundary, resulting in the lower hardness. Furthermore, the changes of hardness during hot rolling could be attributed to two factors. The first factor was the total plastic strain transferred into the

individual layer, which caused an increase in the microhardness for this clad. The second factor was the possibility of softening during hot rolling. HUMPHREYS and HARTLEY [25] reported that increasing the imposed strain could lower the activation energies for recovery and recrystallization. The onset of such processes could have caused the decrease in microhardness for this clad. In this work, the hardness of both the 7050 layer and interface increased during rolling process, indicating that total plastic strain could play more role in changing hardness than softening such as dynamic recovery and recrystallization, while the balance action between plastic strain and softening might result in little change in hardness of 6009 layer during rolling. Interestingly, solution and aging could simultaneously improve the hardness of 7050 alloy layer, interface and 6009 alloy layer, compared to the rolled state. The dominant strengthening mechanisms of the 7050 layer and 6009 layer were precipitation strengthening and solution strengthening. Furthermore, solution and aging could promote the interdiffusion of solute elements Zn, Mg, Cu and Si at the interface, so solution strengthening was deemed to be the primary strengthening mechanism for the hardness improvement at the interface after solution and aging. In addition, the hardness of the 75% HR + SA specimen on the thin side was much lower than that of 55% HR + SA and 65% HR + SA specimens. This lower hardness might be attributed to the occurrence of recovery and recrystallization during solution process because the 75% HR + SA specimen received greater plastic strain before solution than that of 55% HR + SA and 65% HR + SA specimens.

## 4 Conclusions

1) The three-layer 6009/7050/6009 clad slab was successfully prepared by an innovative direct-chill process with the optimized experimental parameters.

2) The clad ratio showed obvious decrease when the homogenized sample was rolled from 80 to 36 mm, and then changed slightly with further rolling.

3) After successive homogenization and hot rolling at hot reduction levels of 55%, 65% and 75%, the content of rodlike Zn-rich phases increased significantly in 7050 alloy layer, meanwhile the Zn-rich phases were dissolved and disappeared after subsequent solution and aging, and the residual phases were only  $\text{Al}_2\text{Cu}$  phases.

4) With the reduction of the rolled samples, the diffusion layer thickness on both thin side and thick side of the clad decreased; however, a significant increase in diffusion layer thickness could be observed after subsequent solution and aging.

5) Solution and aging treatments significantly improved the hardness in 7050 alloy layer, interfaces and 6009 alloy layers of the rolled samples at every level, except the thin side for the 75% hot reduction sample after solution and aging.

## References

- [1] STOLYAROV V V, ZHU Y T, LOWE T C, ISLAMGALIEV R K, VALIEV R Z. Processing nanocrystalline Ti and its nanocomposites from micrometer-sized Ti powder using high pressure torsion [J]. *Materials Science and Engineering A*, 2000, 282: 78–85.
- [2] JIANG H G, VALDEZ J A, ZHU Y T, BEYERLEIN I J, LOWE T C. The strength and toughness of cement reinforced with bone-shaped steel wires [J]. *Composites Science and Technology*, 2000, 60: 1753–1761.
- [3] KOCICH R, MACHÁČKOVÁ A, KUNČICKÁ L, FOJTÍK F. Fabrication and characterization of cold-swaged multilayered Al–Cu clad composites [J]. *Materials and Design*, 2015, 71: 36–47.
- [4] KOCICH R, KUNČICKÁ L, DAVIS C F, LOWE T C, SZURMAN I, MACHÁČKOVÁ A. Deformation behavior of multilayered Al–Cu clad composite during cold-swaging [J]. *Materials and Design*, 2016, 90: 379–388.
- [5] MILLER W S, ZHUANG L, BOTTEMA J, WITTEBROOD A J, SMET P D, HASZLER A, VIREGGE A. Recent development in aluminium alloys for the automotive industry [J]. *Materials Science and Engineering A*, 2000, 280: 37–49.
- [6] WANG Kai, XUE Han-song, ZOU Mao-hua, LIU Chang-ming. Microstructural characteristics and properties in centrifugal casting of SiC<sub>p</sub>/X1104 composite [J]. *Transactions of Nonferrous Metals Society of China*, 2009, 19: 1410–1415.
- [7] SEXTON L, LAVIN S, BYRNE G, KENNEDY A. Laser cladding of aerospace materials [J]. *Journal of Materials Processing Technology*, 2002, 122: 63–68.
- [8] YAN Y B, ZHANG Z W, SHNE W, WANG J H, ZHANG L K, CHIN B A. Microstructure and properties of magnesium AZ31–aluminum 7075 explosively welded composite plate [J]. *Materials Science and Engineering A*, 2010, 527: 2241–2245.
- [9] BEHCET G. Investigation of interface properties and weldability of aluminum and copper plates by explosive welding method [J]. *Materials and Design*, 2008, 29: 275–278.
- [10] AKBARI-MOUSAVI S A A, BATTETT L M, AL-HASSANI S T S. Explosive welding of metal plates [J]. *Journal of Materials Processing Technology*, 2008, 202: 224–239.
- [11] ZIEGELHEIM J, HIRAKI S, OHASWA H. Diffusion bondability of similar/dissimilar light metal sheets [J]. *Journal of Materials Processing Technology*, 2007, 186: 87–93.
- [12] WANG De-qing, SHI Zi-yuan, QI Ruo-bin. Cladding of stainless steel on aluminum and carbon steel by interlayer diffusion bonding[J]. *Scripta Materialia*, 2007, 56: 369–372.
- [13] WANG J, LI Y J, LIU P, GENG H R. Microstructure and XRD analysis in the interface zone of Mg/Al diffusion bonding [J]. *Journal of Materials Processing Technology*, 2008, 205: 146–150.
- [14] KIM S H, KIM H W, EUH K, KANG J H, CHO J H. Effect of wire brushing on warm roll bonding of 6xxx/5xxx/6xxx aluminum alloy clad sheets [J]. *Materials and Design*, 2012, 35: 290–295.
- [15] CHANG H, ZHENG M Y, GAN W M, WU K, MAAWAD E, BROKMEIER H G. Texture evolution of the Mg/Al laminated composite fabricated by the accumulative roll bonding [J]. *Scripta Materialia*, 2009, 61: 717–720.
- [16] ZHANG X P, CASTAGNE S, YANG T H, GU C F, WANG J T. Entrance analysis of 7075 Al/Mg–Gd–Y–Zr/7075 Al laminated composite prepared by hot rolling and its mechanical properties [J]. *Materials and Design*, 2012, 32: 1152–1158.
- [17] WAGSTAFF R B, LLOYD D J, BISCHOFF T F. Direct chill casting of clad ingot [J]. *Materials Science Forum*, 2006, 519–521: 1809–1814.
- [18] SUN Jian-bo, SONG Xiao-yang, WANG Tong-min, YU Ying-shui, SUN Min, CAO Zhi-qiang, LI Ting-ju. The microstructure and property of Al–Si alloy and Al–Mn alloy bimetal prepared by continuous casting [J]. *Materials Letters*, 2012, 67: 21–23.
- [19] JIANG Hui-xue, ZHANG Hai-tao, QIN Ke, CUI Jian-zhong. Direct-chill semi-continuous casting process of three-layer composite ingot of 4045/3004/4045 aluminum alloys [J]. *Transactions of Nonferrous Metals Society of China*, 2011, 21: 1692–1697.
- [20] LIU Ning, JIE Jin-chuan, LU Yi-ping, WU Li, FU Ying, LI Ting-ju. Characteristics of clad aluminum hollow billet prepared by horizontal continuous casting [J]. *Journal of Materials Processing Technology*, 2014, 214: 60–66.
- [21] YAN Guang-yuan, MAO Feng, CHEN Fei, WU Wei, CAO Zhi-qiang, WANG Tong-min, LI Ting-ju. Characteristics evolution of 6009/7050 bimetal slab prepared by direct-chill casting process [J]. *Transactions of Nonferrous Metals Society of China*, 2016, 26: 895–904.
- [22] YAN Guang-yuan, MAO Feng, CHEN Fei, CAO Zhi-qiang, WANG Tong-min. Effect of homogenization annealing on microstructure, composition and mechanical property of 7050/6009 bimetal slab [J]. *Transactions of Nonferrous Metals Society of China*, 2016, 26: 2532–2541.
- [23] CHAUDHARI G P, ACOFF V. Cold roll bonding of multi-layered bi-metal laminate composites [J]. *Computational Materials Science*, 2009, 69: 1667–1675.
- [24] DENG Ying, YIN Zhi-min, HUANG Ji-wu. Hot deformation behavior and microstructural evolution of homogenized 7050 aluminum alloy during compression at elevated temperature [J]. *Materials Science and Engineering A*, 2011, 528: 1780–1786.
- [25] HUMPHREYS F J, HARTLEY M. Recrystallization and related annealing phenomena [M]. 2nd ed. Oxford: Pergamon, 2004.

## 直接冷却铸造法制备的三层 6009/7050/6009 铝合金 复层板坯的变形和热处理能力

闫光远, 毛丰, 曹志强, 李廷举, 王同敏

大连理工大学 材料科学与工程学院 辽宁省凝固控制与数字化制备技术重点实验室, 大连 116024

**摘 要:** 采用一种新的直接冷却铸造方法制备三层 6009/7050/6009 铝合金复层板坯。为了研究该复层板坯的塑性变形和热处理行为, 对铸态 6009/7050/6009 复层板坯先后进行均匀化退火、热轧、固溶和时效处理。实验结果表明, 在最佳的实验参数下, 7050 合金和 6009 合金实现了良好的冶金结合。当对退火态样品进行压下量为 55% 的热轧处理时, 其包覆率明显降低, 但随着压下量的继续增大, 包覆率变化不明显; 当对退火态样品连续进行压下量为 55%、65% 和 75% 的热轧处理时, 棒状富锌相含量明显增加; 随着压下量的不断增大, 扩散层厚度逐渐变小。经过随后的固溶时效处理后, 除热轧压下量为 75% 的样品薄侧外, 三层复层板坯中 7050 合金层、界面层和 6009 合金层的硬度均显著增加。

**关键词:** 铝合金; 三层复层板坯; 直接冷却铸造; 塑性变形; 热处理

(Edited by Wei-ping CHEN)